Supporting Information

"Inhibition of Glycosphingolipid Biosynthesis Induces Cytokinesis Failure"
G. E. Atilla-Gokcumen, A. V. Bedigian, S. Sasse and U. S. Eggert

Supporting Figures:

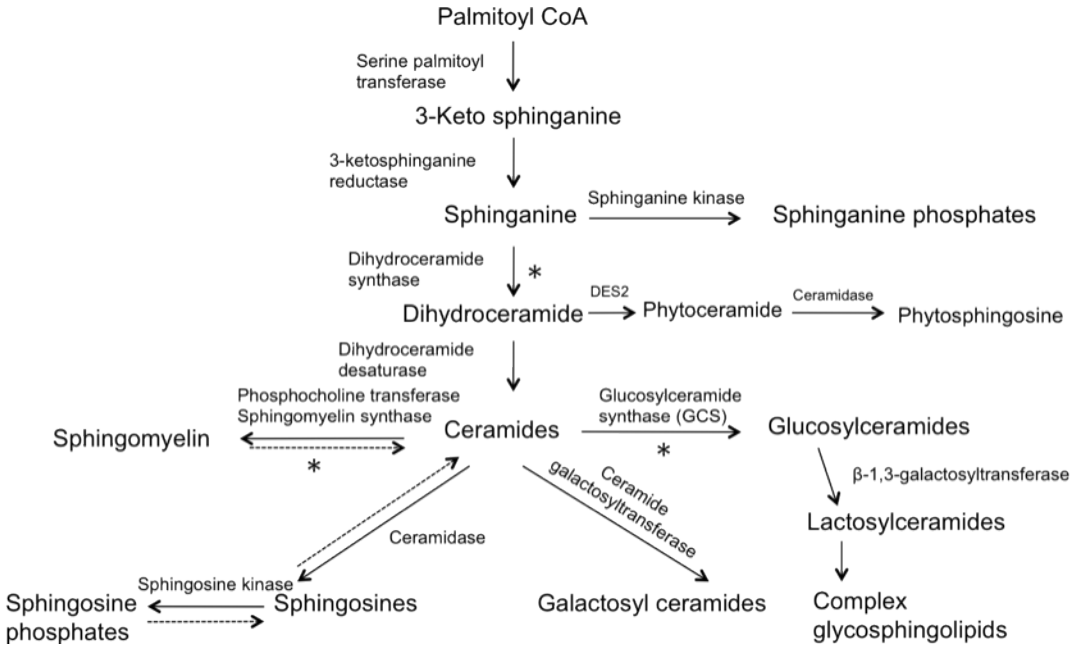

Supporting Figure 1. A simplified version of the sphingolipid biosynthesis pathway. Inhibition of steps marked with an asterisk causes binucleate cell formation. Scheme is adapted from Wennekes *et al.* (2009).[1]

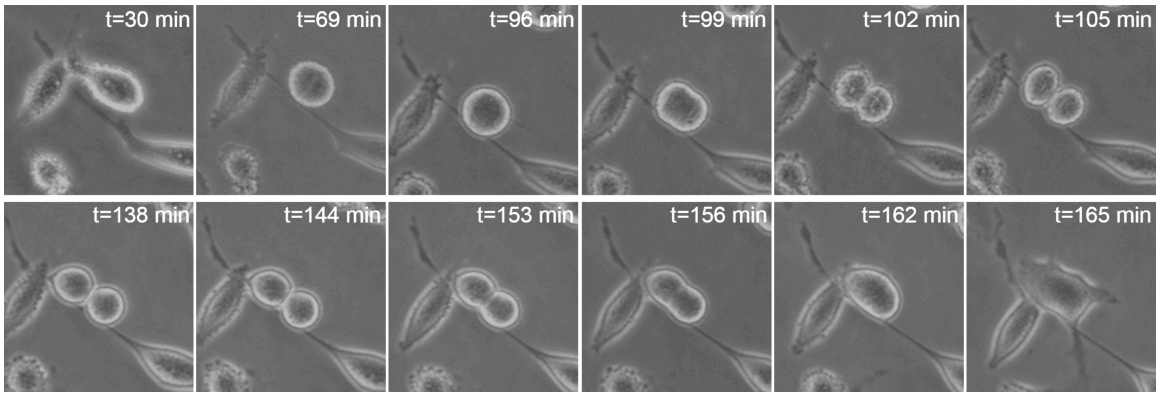

Supporting Figure 2. Live-cell imaging of cells treated with 20 μM PPMP. PPMP was added at t = 0min. Time lapse images were taken every 3 minutes. Representative images are shown here (n = 11 for cells that fail cytokinesis). The cleavage furrow assembles and ingresses, but then cytokinesis fails during ingression (starting at t = 156 min).

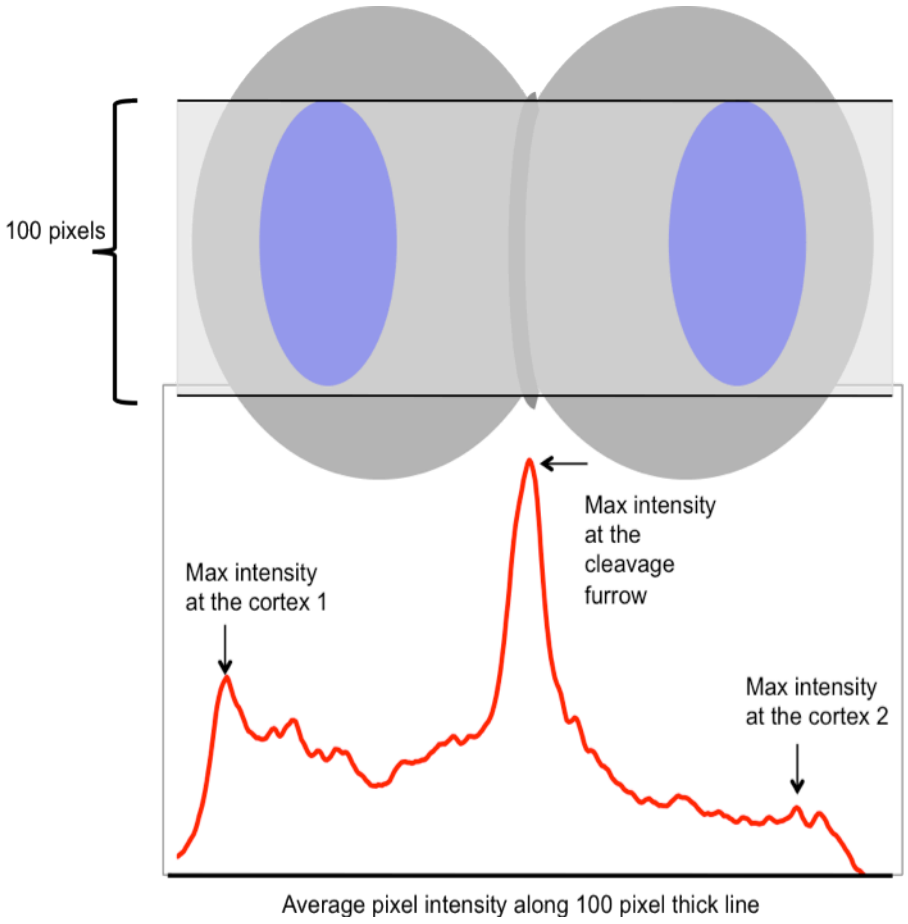

Supporting Figure 3. Cartoon showing the cellular regions used for quantification of furrow localization of ERM. 15 dividing cells were randomly selected based on their tubulin staining. Average pixel intensity of a 100-pixel-thick line drawn across the cleave furrow of a sum projection was calculated in Metamorph. The fold increase at the furrow was calculated by [(Max intensity at the cleavage furrow)/((Max intensity at the polar cortex 1 + Max intensity at the polar cortex 2)/2)]. When there were cell-cell interactions at one cortex, the intensity of the other cortex was used instead of the average. Afterwards, the average cleavage furrow localization was calculated for $n = 15$. In control cells, average ERM localization at the furrow was 1.3x increased at the furrow relative to the poles, which increased to 1.54 with PPMP treatment.

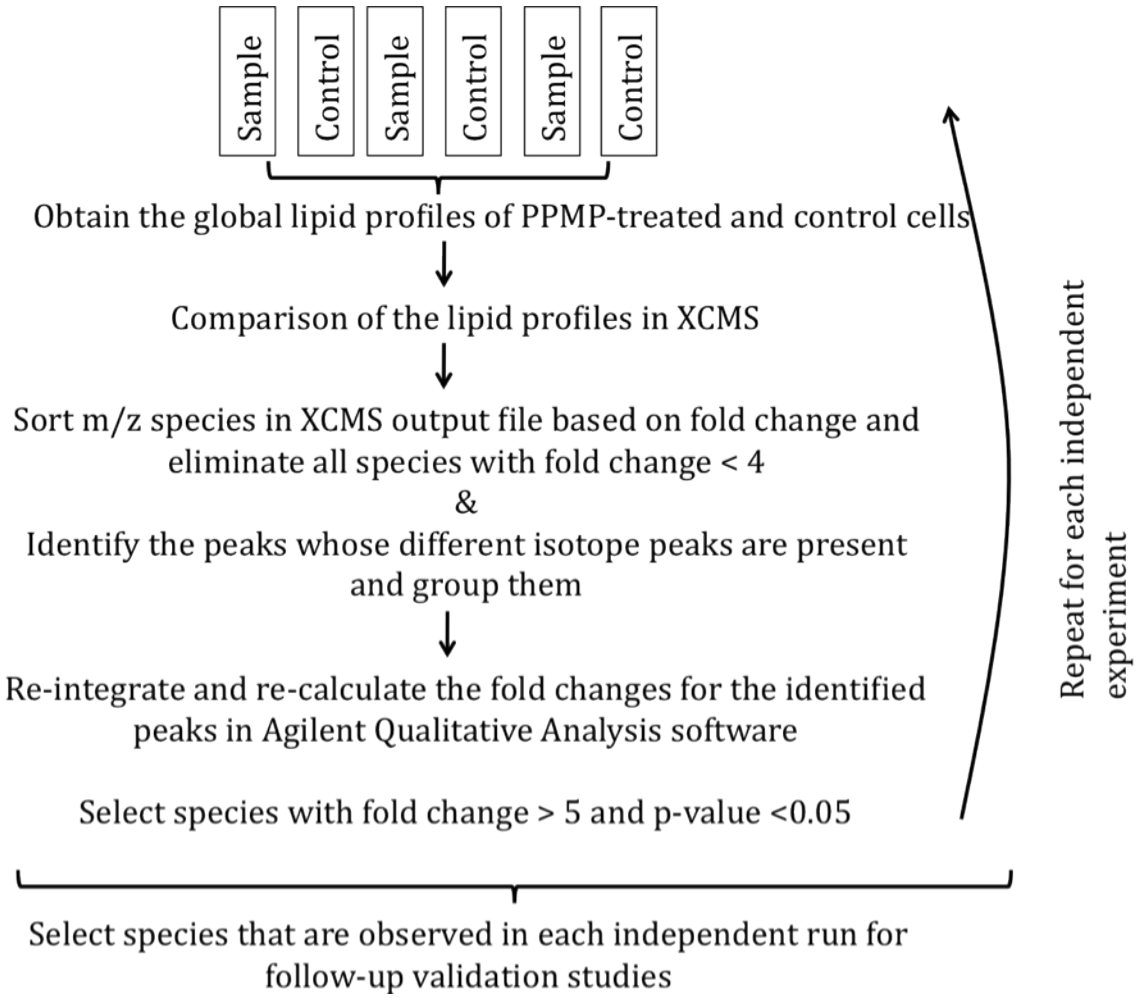

Supporting Figure 4. Summary of workflow to select the hits of the profiling experiments.

Inhibitor	*Target Pathway*	*Target Enzyme*	*Binucleation*
Urb597	fatty acid	fatty acid amide hydrolase inhibitor	No
TOFA	fatty acid	Acetyl CoA	No
Urb602	fatty acid	monoacyl glycerol	Yes (moderate)
ETYA	fatty acid	Inhibits arachidonic acid uptake	No
Terbinafine	cholesterol	squalene epoxidase	No
SDZ-089443	cholesterol	aromatase	No
Cerulenin	cholesterol	HMG-CoA	No
Ezetimibe	cholesterol	Niemann-Pick C1-Like 1 (inhibits cholesterol uptake)	No
Fenretinide	sphingolipid	causes ceramide to build up (retinoid analog)	No
D-erythro MAPP	sphingolipid	alkaline ceramidase	No
L-erythro MAPP	sphingolipid	Negative control	No
L-Cycloserine	sphingolipid	ketosphinganine synthase	No
3-O-Methyl-Sphingomyelin	sphingolipid	neutral sphingomyelinase	Yes (moderate)
N-SMase Spiroepoxide Inhibitor	sphingolipid	neutral sphingomyelinase	No
Epoxyquinone G109 (racemic)	sphingolipid	neutral sphingomyelinase	No
Sphingolactone-24	sphingolipid	neutral sphingomyelinase	No
Manumycin A	sphingolipid	neutral sphingomyelinase	No
GW4869	sphingolipid	neutral sphingomyelinase	No
DL-PDMP	sphingolipid	glucosylceramide synthase	Yes
DL-PPMP	sphingolipid	glucosylceramide synthase	Yes
Conduritol B Epoxide	sphingolipid	glucocerebrosidase	No
MSDH-C	sphingolipid	inhibitor of glycosphingolipid biosynthesis	No
DL-threo-Dihydrosphingosine	sphingolipid	sphingosine kinase	No
D-erythro N,N-Dimethylsphingosine	sphingolipid	sphingosine kinase	Yes (moderate)
Cyclo-propenylceramide	sphingolipid	dihydroceramide desaturase	No
GT-11	sphingolipid	dihydroceramide desaturase	No
AMP-Deoxynojirimycin	sphingolipid	β-glucosidase 2	Yes (moderate)
Myriocin	sphingolipid	serine palmitoyltransferase	No
OGT 918	sphingolipid	glucosylceramide synthase	Yes (weak)
Ceramide Kinase Inhibitor, K1	sphingolipid	ceramide kinase	No
FB1	sphingolipid	ceramide synthase	Yes
FB2	sphingolipid	sphingosine acyltransferase	No
SEW2871	sphingolipid	Sphingosine-1-phosphate receptor 1	Yes (weak)
FTY720	sphingolipid	sphingosine-1-phosphate (S1P) receptors 1,3,4,5	No

Supporting Table 1. Lipid biosynthesis inhibitors that were tested. Compounds, the pathway they target and their specific enzyme targets are shown. The compounds that are highlighted in gray are the 2nd group of inhibitors that target sphingolipid biosynthesis.

m/z	Ret. Time	Levels found to be changing in three independent runs	Fold change	Final m/z species to be validated	Species assigned
365.3434	50 min	Yes	2.7	NO[(1)]	*n/a*
508.4737	70 min	No	*n/a*	NO[(2)]	*n/a*
536.5073	71 min	Yes	10.3	YES	**2**
620.6011	75 min	Yes	8.1	YES	**3**

Supporting Table 2. Initial lipids indentified from PPMP global lipid profiling: Both positive and negative mode of three independent runs were analyzed. After XCMS data was sorted, peaks corresponding to m/z species were manually checked in Agilent Qualitative Analysis software based on their purity and retention time. Peaks were re-integrated manually and species with >5 fold change were determined as the final lipids for the validation experiments.

(1) m/z = 365.3434 was not chosen for further analysis due to the low fold change (2.7).

(2) m/z = 508.4737 was not chosen for further analysis because its accumulation was not observed in all three independent experiments.

m/z	Ret. Time	Present in two independent runs	Fold change (control/sample)	Final m/z species to be validated	Species assigned
659.5568	69 min	Yes	2.6	NO[3]	*n/a*
698.5568	69 min	Yes	11.2	YES	**4**
810.6843	74 min	Yes	6.5	YES	**5**
1136.7903 [2]	68 min	Yes	*n/a* [1]	YES	**6**
1024.6639	63 min	Yes	*n/a* [1]	YES	**7**

Supporting Table 3. Initial lipids indentified from siGCS global lipid profiling: Both positive and negative mode of two independent runs were analyzed. After XCMS data was sorted, peaks corresponding to m/z species were manually checked in Agilent Qualitative Analysis software based on their purity and retention time. Peaks were re-integrated manually and species with >5 fold change were determined as the final lipids for the validation experiments.

[1] Due to the very low abundance of these masses in siGCS-treated cells, the peak areas could not be integrated. Thus, the fold change could not be calculated.

[2] M-OH ion was also observed for this species as a minor peak.

[3] m/z = 659.5568 was not chosen for further analysis due to the low fold change (2.6).

	Molecular Formula	Mass (M-H)	Ret. Time PPMP Profiling / siGCS Profiling	Fold change in PPMP Profiling (PPMP/control)	Fold change in siGCS Profiling (siGCS/control)
Cer(d18:1/2:0)	$C_{20}H_{39}NO_3$	340.2853	*n/a* [1]		
Cer(d18:1/4:0)	$C_{22}H_{43}NO_3$	368.3167	*n/a* [1]		
Cer(d18:1/6:0)	$C_{24}H_{47}NO_3$	396.3480	*n/a* [1]		
Cer(d18:1/8:0)	$C_{26}H_{51}NO_3$	424.3793	*n/a* [1]		
Cer(d18:1/10:0)	$C_{28}H_{55}NO_3$	452.4106	*n/a* [1]		
Cer(d18:1/12:0)	$C_{30}H_{59}NO_3$	480.4419	*n/a* [1]		
Cer(d18:1/14:0)	$C_{32}H_{63}NO_3$	508.4733	70 min / 69 min	2.2	0.7
Cer(d18:1/16:0)	$C_{34}H_{67}NO_3$	536.5079	71 min / 70 min	10.3	0.8
Cer(d18:1/18:0)	$C_{36}H_{71}NO_3$	564.5359	72 min / 71 min	*n/a* [2]	1.3
Cer(d18:1/20:0)	$C_{38}H_{75}NO_3$	592.5672	73 min / 72 min	4.4	1.0
Cer(d18:1/22:0)	$C_{40}H_{79}NO_3$	620.6011	75 min / 74 min	8.1	1.2
Cer(d18:1/24:0)	$C_{42}H_{83}NO_3$	648.6299	77 min / 75 min	1.4	1.3
Cer(d18:1/26:0)	$C_{44}H_{87}NO_3$	676.6612	*n/a* [1]		

Supporting Table 4. Targeted analysis of different ceramide species in PPMP- and siGCS-treated and control cells: Their presence in the lipid extract were evaluated and fold changes were calculated for ceramides that were present. The retention times for the PPMP and GCS RNAi experiments are slightly different because they were done at different times and we replaced the LC/MS column in between the experiments. We always used consecutive runs with each data set so that each data set is internally consistent.

[1] These lipids were either not present in the extract or present at very low levels.

[2] Fold change of Cer(d18:1/18:0) could not be reported because there are other species present in the extracted ion chromatogram which does not allow accurate peak integration.

	m/z observed	Ion obs	retention time	Enhanced /Depleted	Fold change	Species assigned
PPMP	536.5073	M-H	71 min	Enh	10.3	**2**
PPMP	620.6011	M-H	75 min	Enh	8.1	**3**
siGCS	698.5568	M-H	69 min	Dep	11.2	**4**
siGCS	810.6843	M-H	74 min	Dep	6.5	**5**
siGCS	1136.7903	M+H	68 min	Dep	*n/a*[(1)]	**6**
siGCS	1024.6639	M+H	63 min	Dep	*n/a*[(1)]	**7**

Supporting Table 5. m/z species identified as a result of PPMP and siGCS treatment.
[(1)] Due to the very low abundance of these masses in siGCS-treated cells, the peak areas could not be integrated. Thus, the fold change could not be calculated.

Materials and Methods

Cell culture media and supplement were purchased from Sigma and Invitrogen. LC/MS solvents were purchased from Honeywell Burdick&Jackson. Anti-α tubulin (DM1α, T9026) and TRITC-phalloidin (P1951) were purchased from Sigma and anti-ERM was purchased from Abcam. siGCS was purchased from Dharmacon (siGENOME SMARTpool, M-006441-02) and transfection reagent HiPerfect was purchased from Qiagen. LC/MS columns were purchased from Phenomenex (see **LC/MS analysis** section for details). PPMP was purchased from Biomol (Enzo Life Sciences). Lipid species were purchased from Avanti Polar Lipids, except for Cer(d18:1/16:0) (Biomol, Enzo Life Sciences).

Cell Culture. HeLa cells were grown at 37°C in DMEM (Invitrogen) supplemented with 10% fetal bovine serum (FBS) (Sigma) and 1% penicillin/streptomycin (Invitrogen) in 10 cm flasks (Corning).

siGCS treatment. A stock solution of 20 μM of siGCS was prepared in Dharmacon siRNA buffer. 500,000 cells were plated in 10 cm flasks in 7.5 ml DMEM/10% FBS. At the time of plating, siRNA complex was prepared by diluting 40 μL of siGCS stock (to a final concentration of 80 nM) in 2.4 mL OPTIMEM and 75 μL of HiPerfect. siRNA complex was added dropwise to the cells. After 24 hours, the media was replaced with complete media containing P/S. Cells were collected by scraping off after 72 hours and pellets were obtained by centrifugation at 200xg.

PPMP treatment. 900,000 cells were plated in 10 cm flasks and allowed to attach for 24 hours. Afterwards, PPMP was added to a concentration of 10 μM and incubated for an additional 24 hours. Control cells were treated with 1% DMSO. Cells were collected by scraping off and pellets were obtained by spinning down at 200xg.

Preparation of lipid extracts for LC/MS. Cell pellets were resuspended in 1 mL PBS and Dounce-homogenized in 1:1:2 PBS:MeOH:$CHCl_3$. The resulting suspension was centrifuged at 500xg for 10 minutes followed by the separation of the chloroform layer from the aqueous layer. In order to increase the concentration of lipids, samples were evaporated and re-dissolved in 100 μL chloroform.[2]

LC/MS analysis. LC/MS analysis was performed using an Agilent 6520 Series Accurate-Mass Quadrupole Time-of-Flight LC/MS. For the LC/MS analysis in negative mode, a Gemini C18 reversed phase column (50 μm, 4.6 mm x 50 mm) from Phenomenex was used together with a reversed phase guard cartridge (C18, Phenomenex). In positive mode, a Luna C5 reversed phase column (50 μm, 4.6 mm x 50 mm) from Phenomenex was used together with a reversed phase guard cartridge (C5, Phenomenex). Stationary phase A consisted of a 95:5 H_2O:MeOH, and mobile phase B was prepared by 60:35:5 2-propanol:MeOH:H_2O. 0.1 % formic acid and 5 mM ammonium formate for the positive ionization mode, and 0.1 % ammonium hydroxide for the negative ionization mode, were added prior to LC/MS runs.

For each run, the flow rate started at 0.1 ml/min for 5 min to alleviate the backpressure associated with injecting chloroform, followed by a flow rate of 0.5 ml/min for the duration of the gradient. The gradient started after 5 min at 0 % B and then increased to 100 % B over the course of 70 min followed by an isocratic gradient of 100 % B for 8 min before equilibration for 7 min at 0 % B. The total analysis time was 90 min. MS analysis was performed using an Agilent ESI-TOF fitted electrospray ionization (ESI) source. The capillary voltage was set to 3500 V and the fragmentor voltage to 175 V. The drying gas temperature was 350 °C, the drying gas flow rate was 12 L/min and the nebulizer pressure was 30 psi. Untargeted data were collected using a mass range of 100-1700 Da in extended dynamic range mode, and each run was performed using 30 µl injections of HeLa lipid extract. In each run, we analyzed alternating treated and control samples (three each). Multiple (three for PPMP, and two for siGCS) independent experiments were used for final profiling analysis. MS/MS experiments were carried out in a similar fashion, but different collision energies were tested to find the optimal ionization. Fragmentation patterns were observed at 15 V, 35 V and 55 V.

Data Analysis. For lipid profiling, analysis of the resulting total ion chromatograms was performed using the software package XCMS.[3] Files were converted from Agilent Masshunter format to mzXML files with the software "trapper". Treated and untreated samples were compared and ranked according to fold change, peak size and statistical significance.

We carried out several elimination steps to determine which m/z species were significantly changed in the presence of PPMP and siGCS. First, m/z species obtained from XCMS for each run were sorted based on fold change and p value. m/z species with < 4 fold change and p value > 0.05 were eliminated. We also grouped the peaks based on their isotropic distribution because any significant m/z peak should be present with peaks corresponding to other isotopes. Next, we manually investigated the peaks in Agilent Qualitative Analysis software. Well-resolved and pure peaks were reintegrated and fold changes were recalculated manually (see Supporting Table 2 & 3 for the resulting m/z). Once accurate fold changes were calculated based on manual integration, we eliminated species with < 5-fold change. Finally, we compared the presence of m/z species in different runs and looked at the species that were observed in different independent experiments so that we would only carry on the most reproducible m/z species to the validation step (Supporting Figure 4).

Identification and validation of 2 and 3. For m/z 536.5073 and 620.6011, molecular formulas were generated based on high-resolution mass in Agilent Qualitative Analysis software. We performed a search in the LIPIDMAPS database to find the corresponding lipid species based on the molecular weight (M+H) and formula. For 536.5073, we found Cer(d18:1/16:0) and for 620.6011, we found Cer(d18:1/22:0). We then purchased these candidate lipids and compared MS/MS profiles of these lipids and 536.5073 and 620.6011. More specifically, we compared the fragmentation pattern of 536.5073 with Cer(d18:1/16:0) and 620.6011 with Cer(d18:1/22:0). For 536.5089 and Cer(d18:1/16:0), we observed the same fragmentation patterns that the parent mass fragments to 488.4846, 280.2646 and 237.2225 at the same retention times; thus, we assigned 536.5089 to be

Cer(d18:1/16:0) (**2**) (Supporting Table 4). Similarly for 620.6011 and Cer(d18:1/22:0), we observed the same fragmentation patterns that the parent mass fragments to 364.3585, 338.3426, 231.3172 and 237.2225 at the same retention times; thus, we assigned 620.6011 to be Cer(d18:1/22:0) (**3**) (Supporting Table 5).

Identification and validation of 4 and 5. For m/z 698.5568 and 810.6843, we performed a search in the LIPIDMAPS database to find the corresponding lipid species based on the molecular weight (M+H). For 698.5568, we found GlcCer(d18:1/16:0) and for 810.6843, we found GlcCer(d18:1/24:0). We then purchased GlcCer(d18:1/16:0) and GlcCer(d18:1/24:1) (because GlcCer(d18:1/24:0) was not commercially available) and compared MS/MS profiles of these lipids and 698.5568 and 810.6843. More specifically, we compared the fragmentation pattern of 698.5568 with GlcCer(d18:1/16:0) and 810.6843 with GlcCer(d18:1/24:1). For 698.5568 with GlcCer(d18:1/16:0), we observed the same fragmentation patterns that the parent mass fragments to 536.5068, 488.4872, 280.2646, 237.2225, 113.0243 and 101.0242 at the same retention times; thus, we assigned 698.5568 with GlcCer(d18:1/16:0) (**4**) (Supporting Table 5). For 810.6843, we observed, 648.6288, 392.3909, 367.3631, 143.0351, 119.0386, 113.0234 and 101.0245. For GlcCer(d18:1/24:1), we observed the following -2H masses: 646.6153, 390.3714, 365.3414, and the following ions that belong to the same GlcCer backbone: 143.0355, 119.0347, 113.0234 and 101.0247. Thus, we assigned 810.6843 to be GlcCer(d18:1/24:0) (**5**) (Supporting Table 5).

Identification and validation of 6 and 7. For m/z 1024.6639 and 1136.7903, we performed a search based on M-H in the LIPIDMAPS database to find the corresponding lipid species. For 1024.6639, only 3 neutral glycosphingolipids were found: Galα1-4Galβ1-4Glcβ-Cer(d18:1/16:0), Galα1-3Galβ1-4Glcβ-Cer(d18:1/16:0) and Manα1-3Manβ1-4Glcβ-Cer(d18:1/16:0). We eliminated Manα1-3Manβ1-4Glcβ-Cer(d18:1/16:0) because it is unlikely to be found in mammals, since complex sugars are formed from lactosylated-ceramides in the mammalian sphingolipid pathway.[1] Thus, we assigned 1024.6639 to be Galα1-4Galβ1-4Glcβ-Cer(d18:1/16:0) or Galα1-3Galβ1-4Glcβ-Cer(d18:1/16:0) (**7**) (Supporting Table 4). A similar analysis for 1136.7903 led to the assignment of 1136.7903 to be Galα1-4Galβ1-4Glcβ-Cer(d18:1/22:0) or Galα1-3Galβ1-4Glcβ-Cer(d18:1/22:0) (**8**) (Supporting Table 5).

Targeted analysis of other ceramides. In addition to lipids we identified from global lipid profiling, we also looked at the presence and fold changes of other ceramide species, C2- to C26-ceramides. C2- to C12-ceramides and C26-ceramide were absent or observed at very low abundance; thus we focused on C14- to C24-ceramides. To confirm that we were evaluating the correct species, we first looked at the molecular formulas generated based on high-resolution masses in Agilent Qualitative Analysis software. Once we confirmed that the molecular formulas matched the candidate lipids, we purchased Cer(d18:1/14:0), Cer(d18:1/20:0) and Cer(d18:1/24:0) and compared MS/MS profiles and retention times of these lipids to the peaks we observed. More specifically, we compared the retention times and fragmentation patterns of m/z=508.4733 to Cer(d18:1/14:0), m/z=592.5672 to Cer(d18:1/20:0) and m/z=648.6299 to Cer(d18:1/24:0).

For 508.4733 and Cer(d18:1/14:0), we observed the same fragmentation patterns that the parent mass fragments to 209.1892, 237.2206 and 252.2315 at the same retention times; thus, we assigned 508.4733 to be Cer(d18:1/14:0). For 592.5672 and Cer(d18:1/20:0), we observed the same fragmentation patterns that the parent mass fragments to 237.2200, 293.2805, 336.3230 at the same retention times; thus, we assigned 592.5672 to be Cer(d18:1/20:0). For 648.6299 and Cer(d18:1/24:0), we observed the same fragmentation patterns that the parent mass fragments to 237.2216, 366.3706, 392.3857 at the same retention times; thus, we assigned 592.5672 to be Cer(d18:1/20:0).

Immunofluorescence. Cells were grown on covers slips in 24-well plates. The cell culture medium was removed and the cells fixed with 3.7 % formaldehyde in 1x PBS for 20 min. The cover slips were washed with 1x TBSTx blocked for 30 min at room temperature with Ab-Dil (TBSTx +2% BSA +0.1% NaN_3). After transferring the cover slips to dark chambers, the cover slips were washed with the TBSTx and incubated with the primary antibodies for 1 hour or 10 min (phalloidin). The cells were then washed with the according buffer and in case of primary antibodies incubated with the secondary antibody for 1h at room temperature. The cover slips were transferred to an object slide with a drop of ProLong Gold antifade reagent for mounting.

Image Acquisition and Processing. All fluorescent images were recorded on a Nikon Ti inverted microscope equipped with a Perfect Focus System Yokagawa CSU-10 spinning disk confocal unit with 488 nm, 568 nm and 647 nm laser lines at the Nikon Imaging Center at Harvard Medical School. Images were processed in MetaMorph software. Maximum projections are shown in Figure 3 and 4.

Linescans. The fluorescence intensity of ERM at the cortex and cleavage furrow was analyzed using the Linescan function in MetaMorph using sum projections generated from image stacks. Briefly, a 100-pixel wide line was drawn across the cleavage furrow using ERM as a guide. For each point along the line, the average intensity of the 100 pixels was calculated in MetaMorph. The maximum average intensities at the cellular cortex and the cleavage furrow were found in the linescan graph generated in Metamorph. For control and PPMP-treated cells, cleavage furrow localization was calculated by dividing the intensity at the furrow by the average cortex intensity (Max intensity at the cleavage furrow)/((Max intensity at the cortex 1 + Max intensity at the cortex 2)/2). When the cortex intensity was changed due to the interactions with other cells, intensities at the cortex where there are no interactions were used instead of the average.

Supporting references:

(1) Wennekes, T.; van den Berg, R. J.; Boot, R. G.; van der Marel, G. A.; Overkleeft, H. S.; Aerts, J. M. *Angew Chem Int Ed Engl* **2009**, *48*, 8848-69.

(2) Saghatelian, A.; Trauger, S. A.; Want, E. J.; Hawkins, E. G.; Siuzdak, G.; Cravatt, B. F. *Biochemistry* **2004**, *43*, 14332-9.

(3) Ivanova, P. T.; Milne, S. B.; Forrester, J. S.; Brown, H. A. *Mol Interv* **2004**, *4*, 86-96.